Thermotropic liquid crystals from engineered polypeptides

Pesce, Diego

Chapter 3

Solvent-Free Liquid Crystals and Liquids Based on GFP-ELP Fusion Proteins

This chapter has been published as part of:
Kai Liu, **Diego Pesce**, Chao Ma, Michael Tuchband, Min Shuai, Dong Chen, Juanjuan Su, Qing Liu, Jennifer Y. Gerasimov, Anke Kolbe, Wojciech Zajaczkowski, Wojciech Pisula, Klaus Müllen, Noel A. Clark and Andreas Herrmann

Advanced Materials, 27: 2459-2465 (2015)

Abstract

In this work, we tested whether solvent free liquids and liquid crystals based on ELP could include functional proteins able to retain their functionality in the mesophase. The ELP (with 72 negative charges) was fused to a green fluorescent protein (GFP) and the anhydrous ELP-surfactant complex showed to have LC behavior. 2D undulated periodic stripes are detected and the fusion of GFP by genetic engineering does only marginally interfere with the phase forming properties while the fluorescence activity of the fusion protein is maintained in the mesophase. To further test the effect of the length of the charged ELP segment and the structure of the surfactant on the LC properties we produced several variants of negatively charged ELPs of different length (to carry from 9 to 144 negative charges) fused to GFP. Solvent-free GFP-ELP melts with smectic ordered mesophases and isotropic liquids were achieved by forming electrostatic complexes with different positively charged surfactants. Their LC behavior was investigated with DSC, POM, SAXS and WAXS. The lengths of the ELPs and surfactant alkyl chains were found to be extremely important in tuning the physical properties of the fluids. Our findings could lead to the further development of protein TLCs for technological applications including biosensing, biocatalysis and bioelectronics.

3.1 Introduction

The intra- and inter-molecular forces that arise from the presence of water molecules are essential for protein structure and function. Numerous examples of enzymes that retain their native structure and catalytic activity in non-aqueous media have been reported[1-7], and although these solvents contained no bulk water, the presence of strong intra-molecular hydrogen bonds and surface-bound water molecules enclosed in a nonpolar solvent sheath was sufficient to stabilize protein structure and function[8]. Proteins exhibit persistent structures with dimensions that exceed the range of their intermolecular forces, such that liquid–vapor co-existence is unattainable[9]. Therefore, solid-state proteins sublime at low pressures or thermally degrade under ambient conditions, for this reason there are no known liquid proteins in the absence of solvent.

However, recent studies have shown that in bovine β-lactoglobulin protein–ligand interactions, the nature of the active site is preserved inside dry vacuum, suggesting that the degree to which water molecules stabilize protein structures may be overstated[10]. Recently, as mentioned in chapter 1, the group of Mann reported an example of solvent free protein melt based on a stoichiometric ferritin–polymer nanoscale construct with surface modifications[11]. The method utilizes the site-specificity of surface amino acid residues and high degree of uniformity in ferritin molecular architecture to produce a discrete single-component ferritin–polymer conjugate. Electrostatically induced complexation of cationized ferritin comprising several covalently coupled N,N-dimethyl-1,3-propanediamine (DMPA) groups per molecule with anionic polymer surfactants resulted in the formation of a solvent-free LC. With the same strategy, the Mann group reported the production of solvent-less liquids of the dioxygen binding protein myoglobin prepared by thermally induced melting of lyophilized samples of protein–polymer surfactant nanoconjugates produced by electrostatic binding of the cationized biomolecules to the anionic polymer surfactants[12]. Unfortunately, the obtained TLCs were not stable and persist only over a small range of temperature. Moreover, the strategy to obtaining liquid crystals from a protein by modifying biologically or chemically the surface might hamper proper folding or activity of the protein itself. The chemical coupling reaction is usually not straightforward and could lead to polydisperse products. Moreover coupling reactions rely on the availability of functional groups exposed and accessible on the surface (that might be not present in other

proteins). For these reasons, the development of a more general and direct method to produce solvent-free LCs that include functional proteins is amenable.
We have previously shown (in chapter 2) that the combination of negatively charged ELPs with suitably chosen positively charged surfactants, followed by dehydration, can be effectively applied as a simple generic scheme for producing solvent-free thermotropic LCs based on proteins. Genetic engineering as a recombinant protein synthesis technology affords a powerful tool for the synthesis of ELPs with predictable properties and biofunctionality. As we discussed in the previous chapter, engineered ELPs allow fabrication of desired sequences with high molecular weights combined with monodispersity, well-defined structures and chain lengths that are impossible to be achieved by chemical synthesis[13-15]. Moreover, genetic engineering also allows the possibility of fusing these polypeptides to a functional protein.
Here we would like to test whether the negatively charged ELP fusion protein and complex formation with cationic surfactants can be a versatile method for the formation of solvent free LCs of functional proteins. Additionally, the goal of this chapter is to study the effect of the length of the ELP and the nature of the surfactant on the LC behavior of the anhydrous complex.

3.2 Results and Discussion

3.2.1 Production of a E72-GFP fusion protein and experiments for LC formation

To understand whether a functional protein could be fused to negatively charged ELP without changing the LC behavior, we first tested the anionic ELP E72 fused to a green fluorescent protein (GFP), for an additional level of functionality. GFP plus, a variant of enhanced green fluorescent protein (see Figure 16a, b for the nucleotides and amino acids sequences), hereafter named GFP was fused to the previously constructed (see chapter 2) ELP E72. After cloning the GFP-ELP fusion protein GFP-E72 was successfully expressed and characterized by SDS gel electrophoresis and MALDI-TOF mass spectroscopy (Figure 1a,b). The SDS gel gave a band in agreement with the expected product (Figure 1b) and the mass spectrum showed a sharp peak (Figure 1a) corresponding to a mass value of 63992.5 (+/-50) Da, which is very close to the expected one (GFP-E72 = 63978.2 Da) calculated based on

the amino acid sequence (Table 1). The activity of GFP in fusion to ELP E72 was measured and GFP fluorescence did not decrease or shift (Figure 1c), indicating that the long negatively charged ELP segment did not interfere with GFP function. Figure 3a shows a schematic representation of the GFP-E72 fusion protein with the GFP (in green) drawn with its characteristic beta-barrel structure, whereas the ELP is presented as an extended coil without exhibiting a defined secondary or tertiary structure, as was demonstrated previously[16].

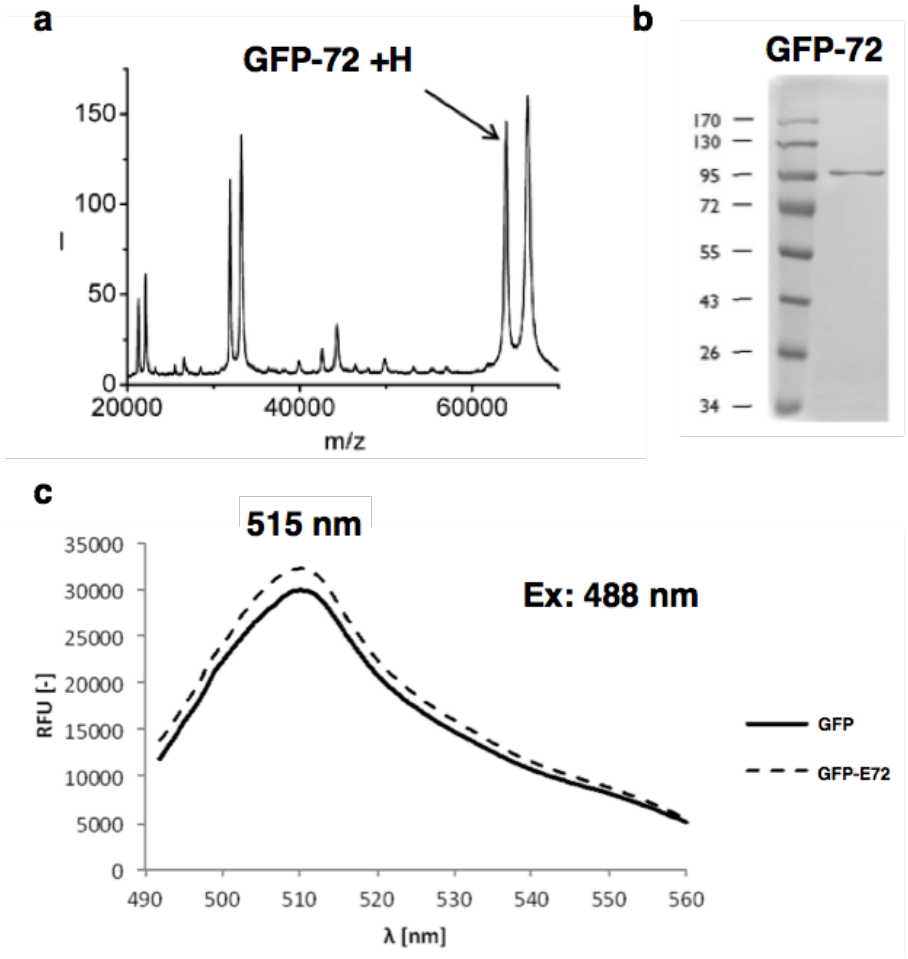

FIGURE 1. CHARACTERIZATION OF GFP-E72. a) MALDI-TOF mass spectrum of GFP-ELP fusion protein GFP-E72; **b)** SDS-PAGE of GFP-E72 which is separated on a 12% SDS-PAGE gel and stained with Coomassie Brilliant Blue R250; **c)** Fluorescence spectra of GFP and GFP-E72 upon excitation at 488 nm.

The complex of GFP-E72 with the surfactant DDAB (Figure 3a) was prepared as described in the previous chapter and its thermal behavior was studied by DSC (differential scanning calorimetry). DSC trace of GFP-E72-DDAB (Figure 2a) is similar to the one of E72-DDAB. DSC scans showed the same two main phase transitions of E72-DDAB complex at 26 and 76 °C (Figure 2a black trace), corresponding to crystalline–smectic and smectic–isotropic transitions, respectively. At 76 °C, the ELP-DDAB complex exhibited an isotropic liquid phase.

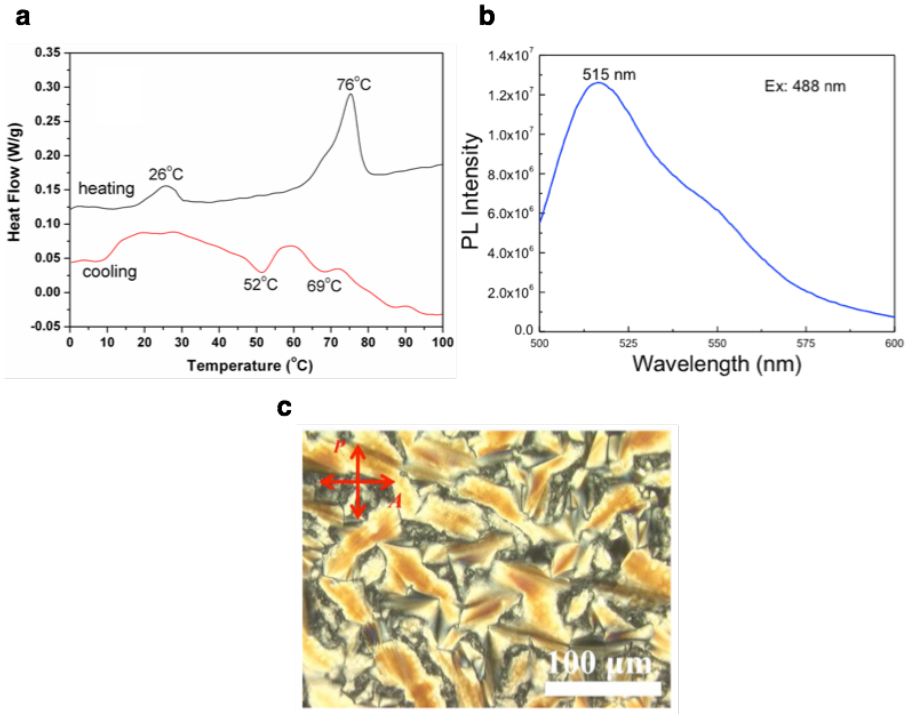

FIGURE 2. CHARACTERIZATION OF GFP-E72-DDAB. a) DSC traces of GFP-E72-DDAB complex upon heating (black line) and cooling (red line) (at a heating/cooling rate of 5 °C/min). DSC of GFP-E72-DDAB is similar to E72-DDAB (see chapter 2); **b)** Fluorescence spectrum of GFP-E72-DDA complex after annealing treatment from isotropic phase to room temperature. Similar fluorescence of GFP and GFP-E72 indicate the stability of GFP in the complex; **c)** Polarized optical microscopy (POM) images of GFP-E72-DDAB complex at 35 °C upon cooling from the isotropic melt to the mesophase in 10 µm thick gaps between glass plates.

Significant differences of the LC behavior were detected for the GFP-E72-DDAB complex compared to the pristine DDAB surfactant (see Figure 3b chapter 2) where DDAB melts at 61 °C, which is around 30 °C higher than the GFP-E72-DDAB complex (see the peak at 26 °C in Figure 2a black trace). After cooling below 60 °C, the peak at around 55 °C indicates the LC

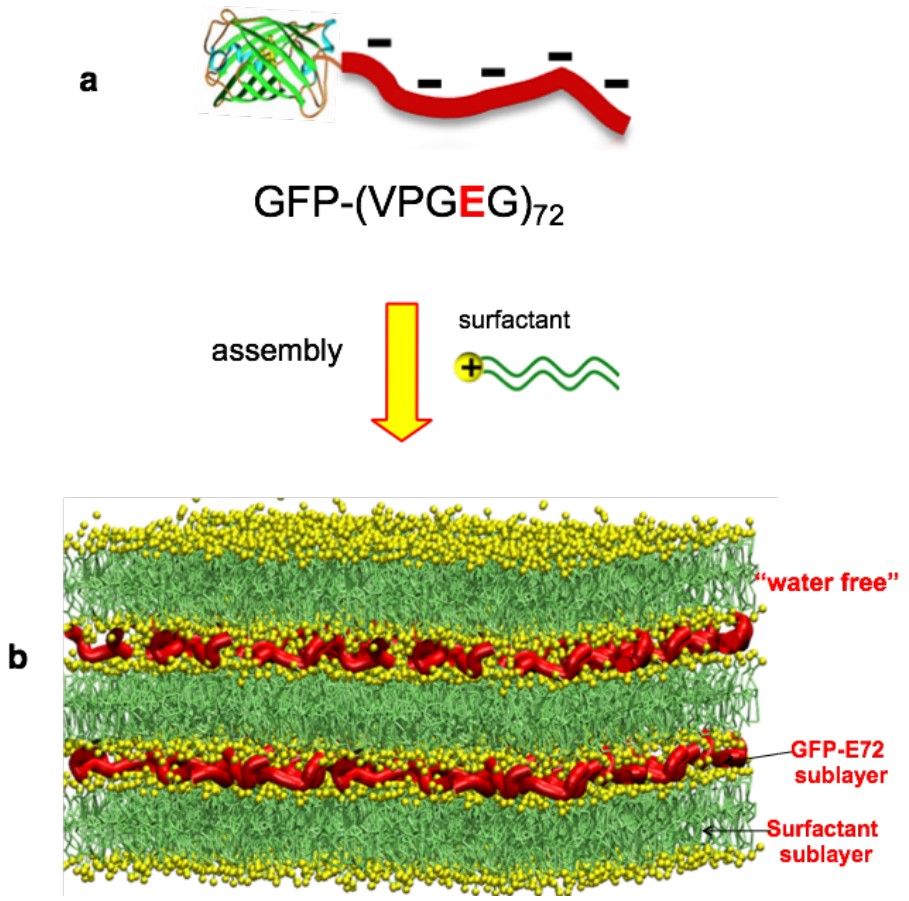

FIGURE 3. SOLVENT-FREE GFP-E72-SURFACTANT COMPLEX. a) Green fluorescent protein (GFP) fused to negatively charged elastin-like polypeptides $(VPGEG)_{72}$ with 72 negative charges GFP-E72; **b)** Proposed lamellar bilayer structure of the liquid crystalline phase. The bilayer structure is made of one sublayer of ELPs and one sublayer of interdigitated surfactants, where the negatively-charged glutamate groups of ELP electrostatically interact with the positively-charged surfactants. GFP residues are randomly penetrated and buried inside the lamellar structures.

transition from a simple smectic phase to a modulated smectic phase (Figure 2a red trace), in agreement with the results of the E72-DDAB complex in the previous chapter.

Upon cooling from isotropic melt at 35 °C, the complex exhibited birefringent focal-conic textures, visualized under the POM (polarized optical microscope) (Figure 2c), indicative of a smectic phase. Figure 2c shows the planar aligned focal-conic domains having the smectic layers locally normal to the glass. The characteristic fluorescent property of GFP was maintained in the mesophase of the GFP-E72-DDAB complex (Figure 2b) indicating that the folded protein was not denatured by the surfactant treatment. Fluorescence spectrum of GFP-E72-DDAB complex in a film after annealing treatment from isotropic phase to room temperature shows unchanged fluorescence properties compared to GFP and GFP-E72, indicating the stability of GFP in the complex (Figure 2 b). On the other hand, it is noteworthy that the GFP did not disturb the mesophase behavior although both components exhibit comparable molecular weights. As for E72, the GFP-E72 complex can be transferred from the TLC to the aqueous phase by treatment with saturated NaCl solution (data not shown). These results, as the ones in the previous chapter, confirm that stable and uniform electrostatic complexes were obtained due to charge-charge interactions, and that at the same time those structures self-assemble into a multilayer architecture (Figure 3b).

Moreover, SAXS and WAXS profiles of the unoriented GFP-E72-DDAB complex at 65 °C confirmed simple smectic phase, with the first and second diffractions (q_1 = 0.248 $Å^{-1}$, q_2 = 0.493 $Å^{-1}$) with repeat distance 25.32 Å (Figure 4 a-c). After cooling below ~ 55 °C, like at 35 °C (Figure 4 d-f), another scattering q value of 0.230 $Å^{-1}$ (red arrow Figure 4 d.) between q_1 and q_2 is observed, which is in agreement with the formation of modulated smectic structures as for E72-DDAB described in chapter 2. This behavior suggests that the GFP-E72-DDAB complex adopts the same structure in the mesophase as E72-DDAB with an Iso-Sm-Smmod phase sequence (see Figure 5b in chapter 2). In addition, no GFP diffraction appeared, indicating random packing of the folded protein in the complex.

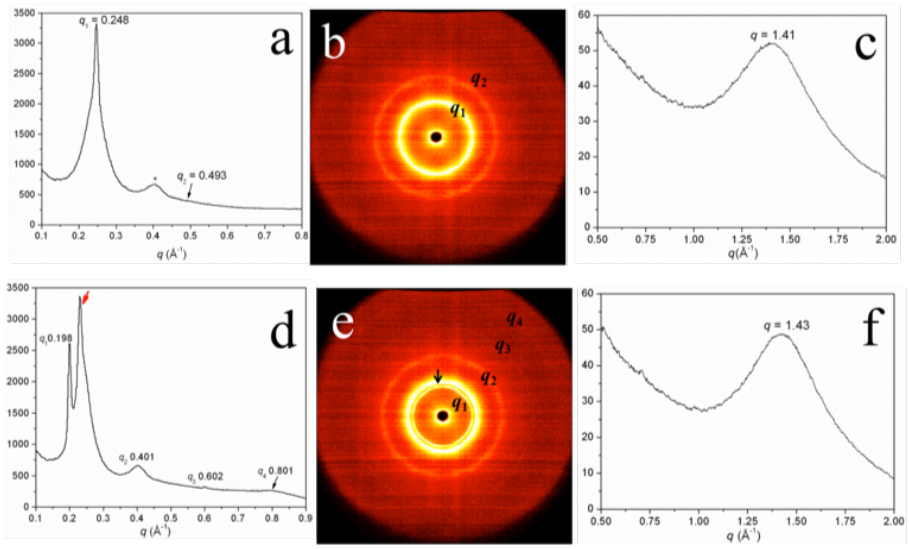

FIGURE 4. SAXS AND WAXS PROFILES OF GFP-E72-DDAB. SAXS and WAXS profiles of the unoriented GFP-E72-DDAB complex at 65 °C **(a-c)** and 35 °C **(d-f)** upon cooling. At 65 °C, simple smectic phase is confirmed by the first and second diffractions (q_1 = 0.248 Å^{-1}, q_2 = 0.493 Å^{-1}) with repeat distance 25.32 Å. After cooling below ~ 55 °C, like at 35 °C, another scattering q value (0.230 Å^{-1}, red arrow) between q_1 and q_2 is observed. The diffraction peak at q~0.4 Å^{-1} (labeled with * in a) is due to the kapton, which is used for sample loading and sealing. In **d**, the 2nd order scattering (q~0.401 Å^{-1}) of E72-GFP-DDAB is overlapped with that of kapton.

3.2.2 Fabrication and characterization of a series of GFP-ELP fusion proteins

After studying the mesophases of GFP-E72-DDAB, two structural parameters of the LC were varied, i.e. the length of the ELP segment and the alkyl chain length of the surfactant, and their influence on the liquid crystalline properties were investigated. Therefore, we created genetically engineered, negatively charged ELPs based on the pentameric repeat sequence (VPGEG)n, of different lengths fused to GFP (Figure 5a). The series of GFP-ELP fusion proteins were generated by recursive directional ligation[17] (see materials and methods) with negative charges ranging from 9 to 144 (GFP-E9, GFP-E18, GFP-E36, GFP-E72 and GFP-E144) (Figure 5a) and subsequently expressed in *E. coli*. Typically, the yield of purified protein was up to 20 mg for a 50 mL of cell culture.

The purity and molecular weights of the products were confirmed by polyacrylamide gel electrophoresis (PAGE) (Figure 5b) and matrix-assisted laser desorption/ionization time-of-flight mass spectrometry (MALDI-TOF MS), respectively (Figure 6). The measured masses were in good agreement with the calculated values based on the amino acid sequences (Table 1).
Fluorescence spectra of GFP, GFP-E9, GFP-E18, GFP-E36, GFP-E72, GFP-E72 and GFP-E144 (Figure 5 c) show that the emission peak of the GFP in the fusion did not change even for the longest ELP tag E144.

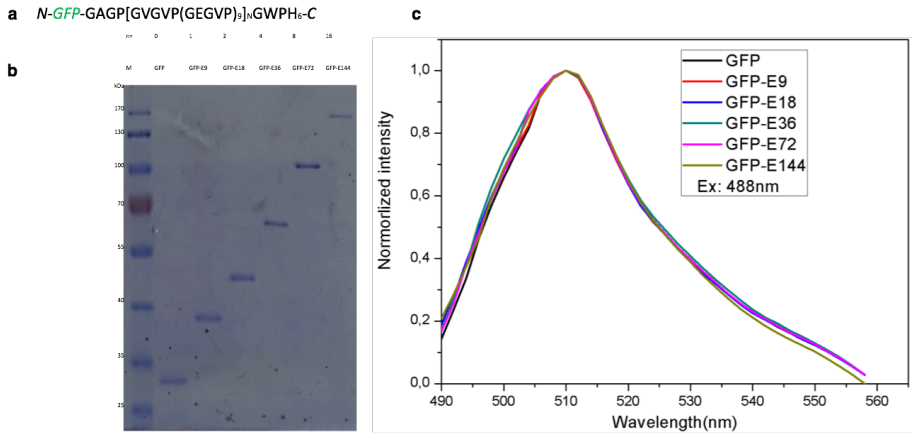

FIGURE 5. CHARACTERIZATION OF GFP-ELP FUSION PROTEINS. GFP fusion variants of negatively charged ELPs. **a)** Amino acid sequence in one letter code of the GFP-ELP fusion protein, where n represents the repeat number of ELP monomers. GFP close to N-terminus is indicated in green; **b)** GFP-ELP fusion proteins separated in a 10% SDS-PAGE and stained with Coomassie Brillinat Blue R250; **c)** Fluorescence spectra of GFP and GFP-ELP variants upon excitation at 488nm.

3.2.3 Preparation and characterization of GFP-ELP complexes with various ELP lengths and different kinds and of surfactants

Solvent-free ELP-surfactant melts were prepared by electrostatic complexation of GFP-ELP (GFP-E9, GFP-E18, GFP-E36, GFP-E72 and GFP-E144) with the following cationic surfactants: dioctyldimethylammonium bromide (DOAB), didecyldimethylammonium bromide (DEAB) and didodecyldimethylammonium bromide (DDAB). Ternary complexes (GFP-ELP-xDOAB-yDEAB, GFP-ELP-xDOAB-yDDAB and GFP-ELP-xDEAB-yDDAB, x+y=1) were also fabricated. The letters x

and y denote the fraction of the respective surfactant complexed to GFP-ELP assuming a ratio of surfactant to glutamate of 1:1. After lyophilization, we investigated the thermal behavior of the protein-surfactant complexes.

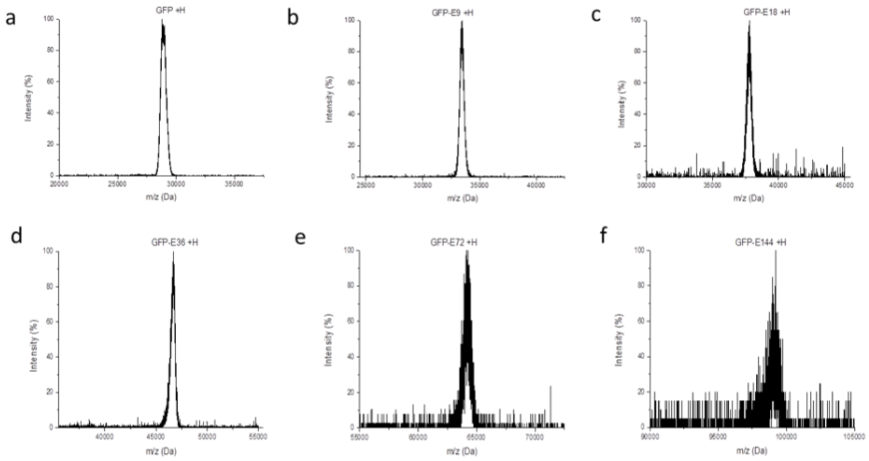

FIGURE 6. MALDI-TOF MASS SPECTRA OF GFP-ELP FUSION PROTEINS. a) GFP; **b)** GFP-E9; **c)** GFP-E18; **d)** GFP-E36; **e)** GFP-E72; **f)** GFP-E144.

TABLE 1. MASS DETERMINATION OF GFP-ELP VARIANTS. *average molecular weight calculated with ProtParam tool. #molecular weight determined by MALDI-TOF mass spectrometry.

Construct	M calc* [Da]	M ms# [Da]
GFP	29060.6	29060.5+/-50
GFP-E9	33425.3	33431.5+/-50
GFP-E18	37790.0	37791.9+/-50
GFP-E36	46519.4	46515.6+/-50
GFP-E72	63978.2	63992.5+/-50
GFP-E144	98895.8	98893.2+/-100

Thermogravimetric analysis (TGA) showed that the complexes had a water content of less than 3% (wt), and that the fluids were thermally stable over a wide range of temperatures until decomposition occurred at around 200 °C (Figure 7a). The results of differential scanning calorimetry (DSC) analysis showed two endothermic peaks on heating corresponding to the phase transitions of crystal–smectic liquid crystal and smectic liquid crystal–isotropic liquid, respectively (Figure 7b-d).

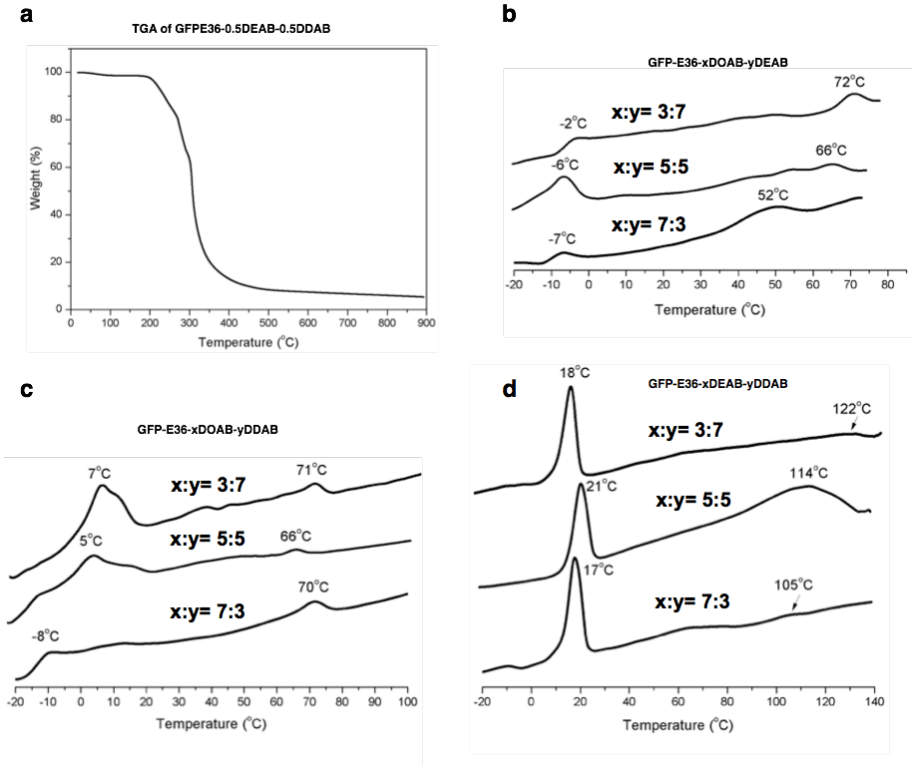

FIGURE 7. CALORIMETRIC ANALYSIS OF GFP-ELP-SURFACTANT COMPLEXES. a) Representative TGA analysis of solvent-free GFP-ELP-surfactant complexes (here, GFP-E36-0.5DEAB-0.5DDAB as an example), indicating that the thermal degradation starts from around 200°C; **b, c, d)** DSC analysis of solvent-free GFP-ELP-surfactant complexes with surfactants of different aliphatic chain lengths (here, GFP-E36 as the example combined with different surfactant mixtures). The traces represent the second heating cycle. Heating rate was 5°C/min; **b)** GFP-E36-DOAB-DEAB system; **c)** GFP-E36-DOAB-DDAB system; **d)** GFP-E36-DEAB-DDAB system. The curves indicate that phase transition temperatures of ELP complexes can be controlled over a wide range.

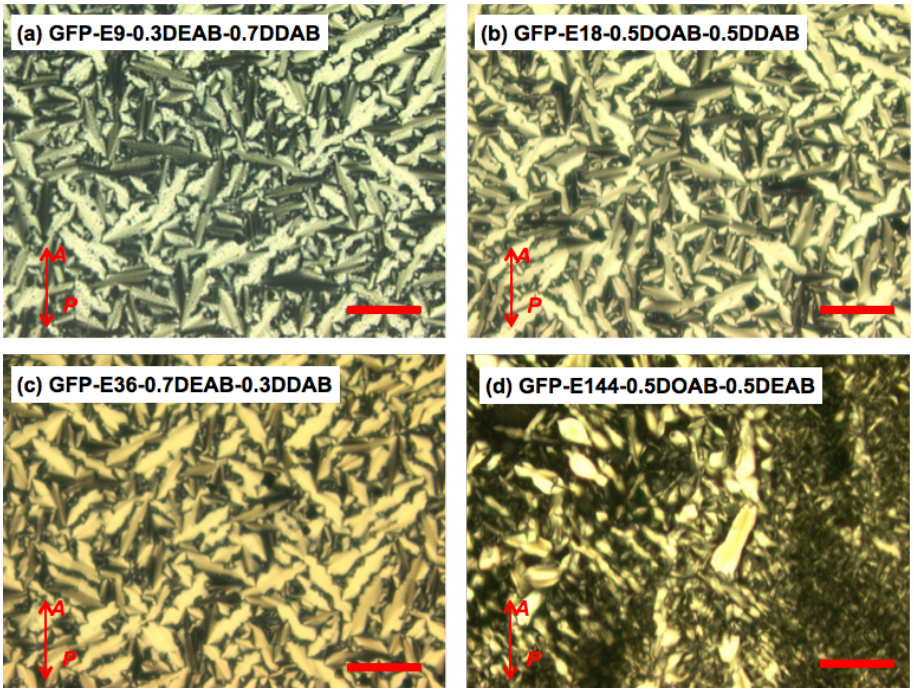

FIGURE 8. POM IMAGES OF GFP-ELP-SURFACTANT COMPLEXES. Representative polarized optical microscopy (POM) images of solvent-free GFP-ELP-surfactant liquid crystals at 25°C. Typical focal-conic textures characteristic of smectic lamellar structures were observed (scale bar is 100 μm).

POM

These phases have been confirmed by polarized optical microscopy (POM) analysis. POM images of the mesophases formed by the GFP-ELP-surfactant complexes (Figure 8) show typical focal-conic textures, characteristic of smectic layer structures. When heated above the clearing temperatures, the birefringent textures completely disappear and the GFP-ELPs-surfactant complexes become isotropic melts (Figure 9).

As summarized in table 2, we found that the short GFP-ELPs (GFP-E9 and GFP-E18) can form stable mesophases only when they were complexed with surfactants of longer alkyl chains. This indicates that longer surfactants effectively prevent the aggregation of the short GFP-ELP with fewer charged groups and promote the self-assembly of the complexes into lamellar structures. Conversely, for the long and more charged ELPs (GFP-E36, GFP-E72 and GFP-E144), all the used surfactants enable the mesophases. While

forming these mesophases, the characteristic fluorescence property of GFP was maintained indicating that the folded protein was not denatured by the surfactant treatment (Figure 10).

TABLE 2. SUMMARY OF MESOMORPHIC BEHAVIOR OF GFP-ELP-SURFACTANT COMPLEXES. Summary of the mesomorphisms of GFP-ELP (GFP-E9, GFP-E18, GFP-E36, GFP-E72 and GFP-E144) complexed with binary surfactant mixtures of different molar ratio ranging from 7:3, 5:5 to 3:7. (x represents no liquid crystal formation, √ represents liquid crystal formation).

	DOAB+DEAB			DOAB+DDAB			DEAB+DDAB		
	(7:3	5:5	3:7)	(7:3	5:5	3:7)	(7:3	5:5	3:7)
GFP-E9	x	x	√	x	√	√	√	√	√
GFP-E18	x	√	√	√	√	√	√	√	√
GFP-E36	√	√	√	√	√	√	√	√	√
GFP-E72	√	√	√	√	√	√	√	√	√
GFP-E144	√	√	√	√	√	√	√	√	√
Surfactant	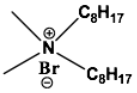 DOAB			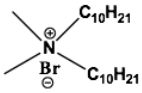 DEAB			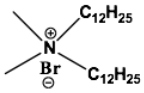 DDAB		

The mesomorphic behaviors of the GFP-ELP-surfactant complexes are summarized in figure 11, exemplified with GFP-E36 complexed with different surfactants. Phase transition temperatures can be controlled over a wide range. Melting points are tunable from about -10 to 25 °C and clearing points are broadly dispersed between 55 and ~120 °C, indicating that the cooperative electrostatic interactions between negatively charged ELP and cationinc surfactants are very important for preventing the aggregation of ELP and stabilizing the mesophases and isotropic liquid phases.

We found a correlation of the phase transition temperatures with the structure of the surfactant. When the length of aliphatic chains increased, the melting and clearing points are generally higher in relation to ELPs complexed with surfactants of shorter alkyl chains. This suggests that van der Waals interactions between adjacent alkyl chains of surfactants represent the dominant intermolecular force determining the thermal behavior[18-20]. When a given surfactant is complexed with different GFP-ELPs, i.e. GFP-E9, GFP-

E18, GFP-E72, GFP-E144, the observed melting and clearing points are similar to those of the GFP-E36 complex. The thermal properties are marginally influenced by varying the ELP segment length. Thus, the length of flexible alkyl chains of surfactant dominates the phase transition behavior of the GFP-ELP-surfactant complexes.

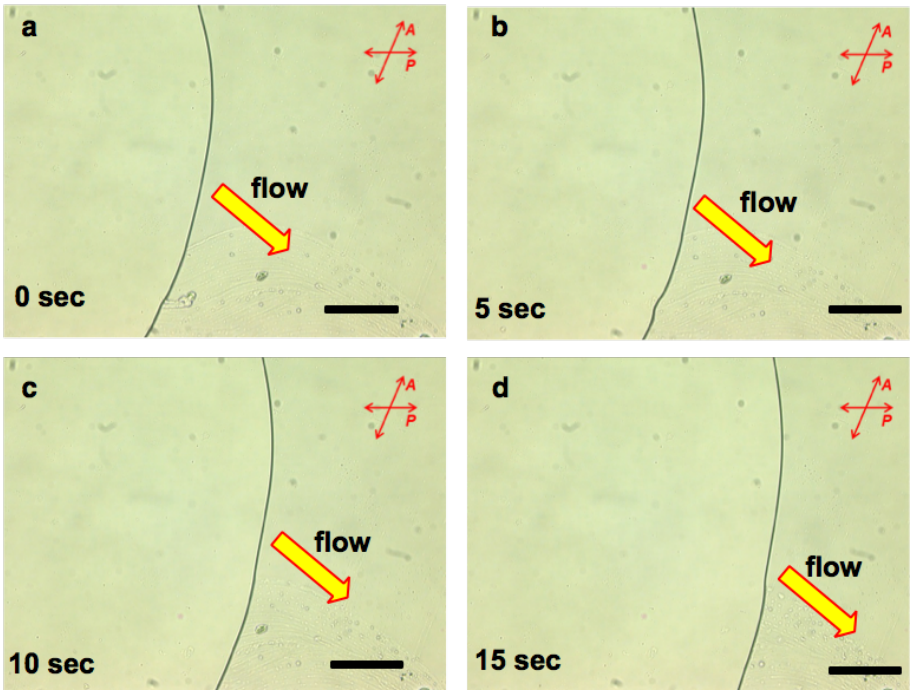

FIGURE 9. POM IMAGES OF GFP-ELP-SURFACTANT COMPLEXES IN ISOTRPIC PHASE. A series of depolarized optical microscopy images of solvent-free GFP-ELP-surfactant complexes after heating into isotropic liquid phases exhibiting Newtonian fluid behavior (here, GFP-E36-0.5DOAB-0.5DEAB at 65°C as an example, scale bar is 100 μm).

SAXS

Subsequently, the intrinsic long range ordered structural features of (GFP-ELP)-surfactant fluids were analyzed by small-angle X-ray scattering (SAXS). In the mesophases, the sharp first order reflection peaks and their harmonics are characteristic of long-range ordered lamellar structures (Figure 12a). Interestingly, elongation of the surfactant alkyl chain leads to a clear shift in the first-order reflections (from 0.29 to 0.23 $Å^{-1}$), corresponding to the layer spacing increasing from 21.6 to 27.3 Å. When the GFP-ELPs with different

lengths (GFP-E9, GFP-E18, GFP-E36, GFP-E72 and GFP-E144) were complexed with a given surfactant, lamellar distances remained the same (Figure 13).

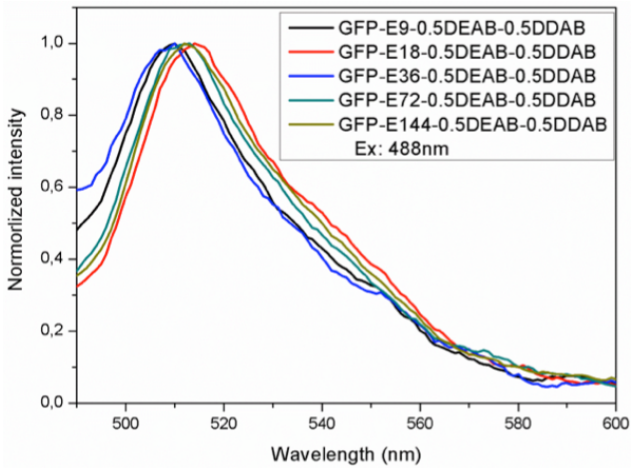

FIGURE 10. GFP FLUORESCENCE SPECTRA IN LC. Fluorescence spectra of representative GFP-ELP-surfactant liquid crystals upon excitation at 488 nm (at 25 °C) indicating that the characteristic fluorescent properties of GFP were maintained in the solvent-free mesophases.

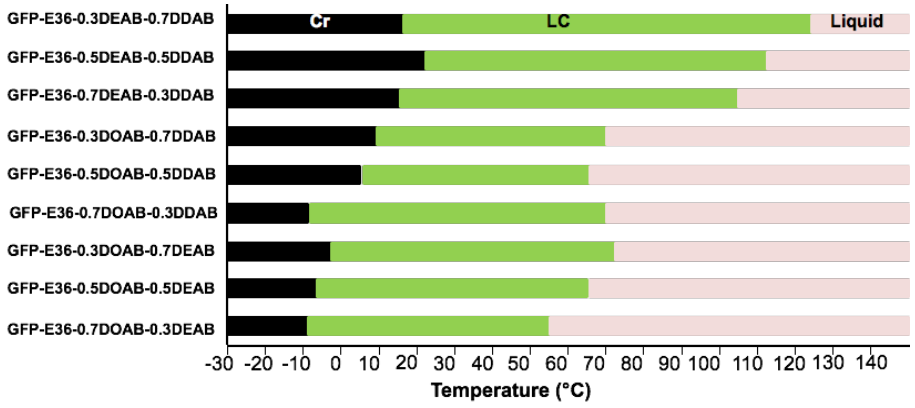

FIGURE 11. SUMMARY OF TEMPERATURE DEPENDENT PHASES OF GFP-ELP WITH DIFFERENT SURFACTANTS. Phase diagram of the GFP-ELP-surfactant complexes exemplified for GFP-E36 complexed with different binary surfactant mixtures. The isotropic-smectic transition and the smectic-crystal transition strongly depend on the length of the aliphatic chains of the surfactants.

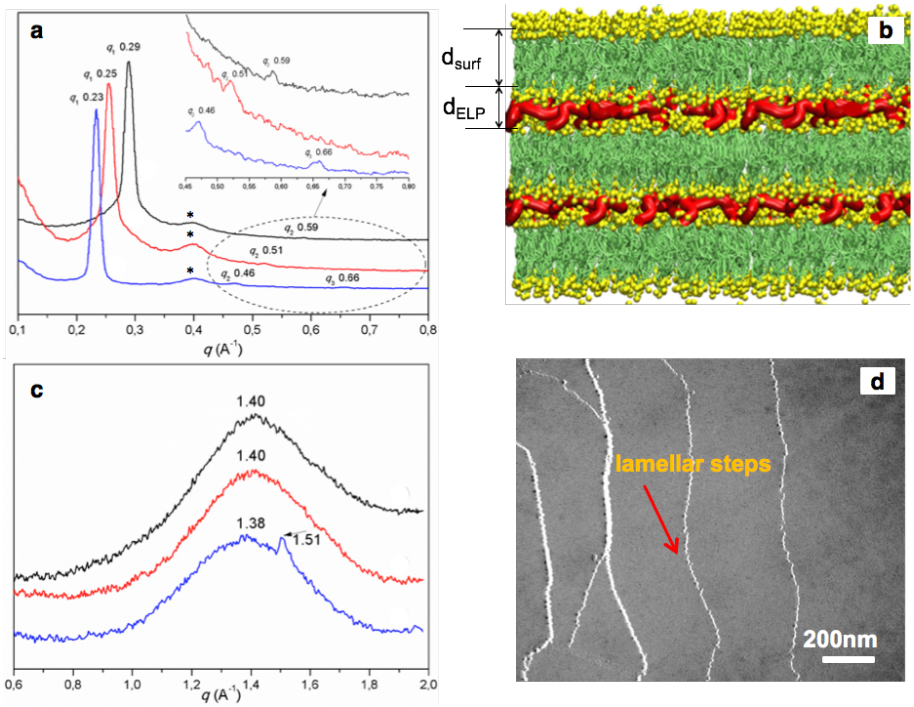

FIGURE 12. STRUCTURAL ANALYSIS OF THE GFP-ELP-SURFACTANT LIQUID CRYSTALS. a) Representative small-angle x-ray scattering profiles of the first order reflections and their harmonics (25°C, black curve, GFP-E36-0.7DOAB-0.3DEAB; red curve, GFP-E36-0.5DOAB-0.5DDAB; blue curve, GFP-E36-0.3DEAB-0.7DDAB) indicating long-range ordered smectic liquid crystal phases. The broad diffraction peak at q~0.4 $Å^{-1}$ (labeled with * in a) is due to the kapton, which is used for sample loading and sealing; **b)** The corresponding model of lamellar molecular organizations (side view) suggesting the anhydrous smectic phases that result in ELP sublayers intercalated between aliphatic hydrocarbon sublayers where GFP residues are randomly packed between the alternating layers; **c)** Wide-angle x-ray scattering profiles of the GFP-ELP-surfactant liquid crystals (25°C, black curve, GFP-E36-0.7DOAB-0.3DEAB; red curve, GFP-E36-0.5DOAB-0.5DDAB; blue curve, GFP-E36-0.3DEAB-0.7DDAB), indicating the intralayer packing of the surfactant alkyl tails; **d)** Freeze-fracture transmission electron microscopy image of the GFP-ELP-surfactant mesophase (GFP-E36-0.3DEAB-0.7DDAB at 60 °C) showing a smooth layer surface and distinct layer steps.

This indicates that the lamellar spacing of the GFP-ELPs mesophase can be manipulated by choosing surfactants with the appropriate alky chain length. In addition, no peak from the GFP moieties packing was observed in the SAXS measurements, which suggests that the fused GFPs are randomly packed without any positional or orientational order. From the dimensions of the ELP and the surfactants, we propose that the smectic lamellar structures consist of

alternating sublayers of ELP of ~10 Å thickness and interdigitated surfactants of ~11.6–17.3 Å thickness, depending on the selected surfactant, and where GFP residues are randomly packed and buried in the lamellar structures (Figure 3b and 12b). Each repeating layer consists of tail-to-tail interacting cationic surfactants which electrostatically interact with the anionic ELP.

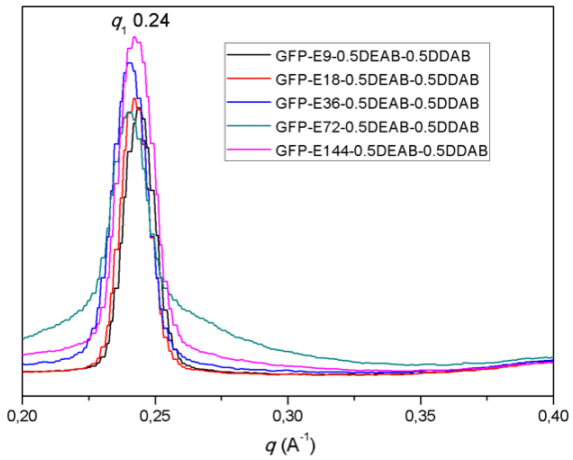

FIGURE 13. SAXS PROFILES OF GFP-ELP-SURFACTANT. SAXS profiles of a series of GFP-ELP melts (GFP-E9, GFP-E18, GFP-E36, GFP-E72 and GFP-E144) complexed with the same surfactants. All the sharp first order reflection peaks appear at 0.24 Å^{-1} corresponding to a layer distance of about 26.2 Å.

Furthermore, SAXS analysis of the GFP-ELP-surfactant melts in the isotropic liquid state showed either no diffraction or only one very broad and weak halo at 0.27 Å^{-1} associated with disordered GFP-ELP-surfactant scattering (23.2 Å) (Figure 14a).

WAXS

Short range alignment of the ELP-surfactant liquid crystals was investigated by wide-angle X-ray scattering (WAXS) (Figure 12c). When the alkyl chain lengths of surfactants are short, only one broad peak at around 1.40 Å^{-1} is observed, corresponding to the typical distance of ~4.5Å between neighboring alkyl chains[11,21,22]. When increasing the lengths of alkyl chains, WAXS profiles exhibit two reflections at 1.38 Å^{-1} and 1.51 Å^{-1}, indicating the ordered intralayer packing of the molten alky chains. WAXS gave another broad halo at ~1.40 Å^{-1}, which corresponds to the average distance (4.5 Å) between the liquid-like aliphatic chains (Figure 14b).

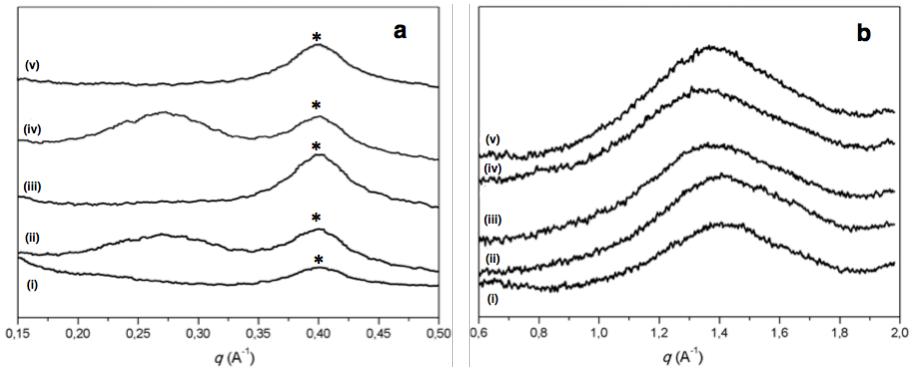

FIGURE 14. SAXS AND WAXS OF GFP-ELP-SURFACTANT IN THE ISOTROPIC PHASE. SAXS **a)** and WAXS **b)** profiles of solvent-free GFP-ELP-surfactant complexes in the isotropic liquid phases (i) GFP-E9-0.5DEAB-0.5DDAB at 130°C; (ii) GFP-E18-0.5DOAB-0.5DDAB at 110°C; (iii) GFP-E36-0.5DOAB-0.5DEAB at 80°C; (iv) GFP-E72-0.5DEAB-0.5DDAB at 130°C; and (v) GFP-E144-0.5DOAB-0.5DEAB at 80°C). Only one broad halo appeared at 0.27 $Å^{-1}$ in SAXS and 1.4 $Å^{-1}$ in WAXS confirming the disordered GFP-ELP-surfactant complex scattering and intralayer packing of aliphatic chains, respectively. The broad diffraction peak at q~0.4 $Å^{-1}$ (labeled with *) is due to the kapton, which is used for sample loading and sealing.

FF-TEM

Moreover, the topography of the lamellar structure fractured in the bulk was directly visualized by freeze-fracture transmission electron microscopy (FF-TEM) (Figure 12d and 15). Flat and smooth layer surface of GFP-ELPs-surfactant liquid crystals exhibit long-range ordering and are separated by distinct and continuous steps, thus confirming the presence of typical smectic layer ordering.

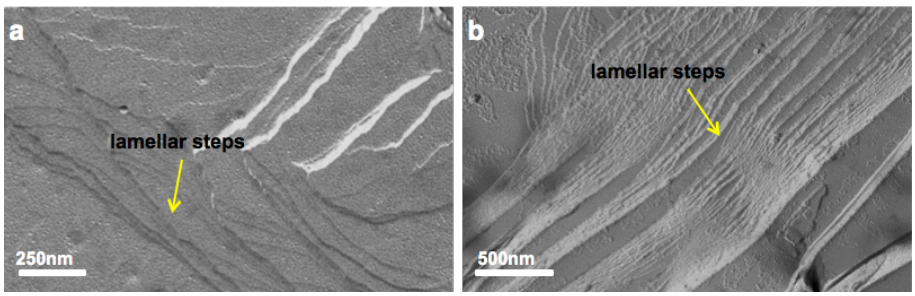

FIGURE 15. FF-TEM OF GFP-ELP-SARFACTANT COMPLEXES. Freeze-fracture transmission electron microscopy images of the GFP-ELP-surfactant mesophases of **a)** GFP-E72-0.5DOAB-0.5DEAB at 25°C and **b)** GFP-E36-0.5DEAB-0.5DDAB at 25°C showing a smooth layer surface and distinct layer steps.

3.3 Conclusion

In conclusion, we have successfully developed a collection of solvent-free GFP functionalized elastin-like protein LCs and liquids by electrostatic complexation of GFP-ELP fusion proteins with different surfactants containing flexible alkyl chains. Electrostatic interactions were found to couple these GFP-ELPs and surfactants into hybrid assemblies, where flexible alkyl chains of surfactants suppress crystallization. The GFP maintained the characteristic fluorescence indicating that the folded protein part was not denatured by the surfactant treatment. The lengths of the ELP and surfactant were found to be extremely important in tuning the physical properties of the fluids. Short GFP-ELP fusion proteins did not form LCs unless complexed with surfactants with longer alkyl chains. By tuning the aliphatic chain length of the surfactants to change the intermolecular alkyl tail-tail forces in the complexes, melting and clearing temperatures of the GFP-ELP-surfactant fluids could be controlled over a broad temperature range. Fluid GFP-ELP was already achieved at temperatures as low as -10 °C, and the transition from the crystal to the liquid crystal can be adjusted up to 25 °C. The liquid crystal to isotropic liquid-transition can be tuned between 55 and 120 °C by selection of the appropriate surfactants. Their high thermal stability (up to 200 °C) can meet a wide range of temperature requirements for technological applications of the fluid ELP without thermal degradation. Hence, the present study of solvent-free GFP-ELP based LCs as a new type of soft biomaterials, where activity of the protein is kept in the solvent-free mesophase, paves the way for potential technological applications in tissue engineering, drug delivery and liquid crystal devices.

3.4 Experimental Section

3.4.1 Materials

E. coli XL1-Blue competent cells were purchased from Stratagene (La Jolla, CA). The pUC19 cloning vector, restriction endonucleases (EcoRI, HinDIII PflMI, BglI, XbaI, NdeI and SacI,), T4 DNA ligase (LC), Fast APTM thermosensitive alkaline phosphatase (Fast AP), and GeneJETTM Plasmid Miniprep kit were purchased from Fermentas (St. Leon-Rot, Germany). Digested DNA fragments were purified using QIAquick® spin miniprep kits from QIAGEN, Inc. (Valencia, CA). The pET-25b(+) vector and E.coli BLR(DE3) competent cells were purchased from Novagen Inc. (Milwaukee, WI). Oligonucleotides were synthesized by biomers.net (Ulm, Germany). BactoTM tryptone and BBLTM yeast extract were purchased from Becton, Dickinson and Co. (Sparks, MD). Potassium phosphate monobasic, potassium phosphate dibasic, sodium phosphate monobasic, sodium phosphate dibasic, sodium chloride, and glycerol were purchased from Merck KGaA (Darmstadt, Germany). Ampicillin and imidazole were purchased from Roth (Karlsruhe, Germany). Isopropyl ß-thiogalactopyranoside (IPTG) was purchased from Duchefa (Harlem, Netherlands). Sinapinic acid matrix and agarose gel were purchased from Sigma-Aldrich (St. Louis, MO) Internal standards bovine serum albumin and trypsinogen were purchased from LaserBio Labs (Sophia-Antipolis, France).

Surfactants used for the GFP-ELPs complex formation dioctyldimethylammonium bromide (DOAB) and didodecyldimethylammonium bromide (DDAB) were purchased from ABCR (Germany), and didecyldimethylammonium bromide (DEAB) was from Sigma–Aldrich.

All chemicals were used as received without any further purification. Ultrapure water, resistivity > 18.2 MΩ·cm, was used for all experiments.

3.4.2 Methods

Cloning and gene oligomerization

The building block of the anionic ELP gene (E9) was ordered from Entelechon (Regensburg, Germany) and was delivered in the pEN vector.

ELPs gene oligomerization was performed as described in chapter 2 and by

Chilkoti and co-workers[17]. Genes of correct length were identified by gel electrophoresis following plasmid digestion with EcoRI and HinDIII and by sequencing (ServiceXS, Leiden, The Netherlands).

Expression vector construction

The expression vector pET 25b(+) was modified by cassette mutagenesis, for incorporation of a unique SfiI recognition site and an affinity tag consisting of six histidine residues at the C-terminus, as described in chapter 2.

FIGURE 16. GFP AMINO ACIDIC AND NUCLEOTIDE SEQUENCE. Nucleotide sequence **a)** and amino acid one letter code **b**) of the green fluorescent protein variant used in this study.

For GFP-ELP fusion protein, the modified pET-SfiI-H6 vector was further digested with XbaI and NdeI, dephosphorylated and purified using a microcentrifuge spin column kit. The gfp gene including the ribosomal binding site was excised from the pGFP vector (pGFP was a kind gift from Prof. D. Hilvert, Federal Institute of Technology, Zurich, Switzerland) (Figure 16a,b) by digestion with XbaI and SacI, and the excised gene (747 bp) was purified by DNA extraction from agarose gel after electrophoresis. A linker sequence that would connect GFP gene and the SfiI restriction site was constructed in the following way: Oligonucleotides, linker_sens (cggtgtagtc ggtttagttc ccagaggaag tca) and linker_antisens (tatgacttcc tctgggaact aaaccgacta caccgagct), both 5'-phosphorylated, were annealed to form a DNA duplex, which contained overhangs corresponding to a SacI and an NdeI

restriction site, respectively. pET-SfiI-H6, the insert containing gfp and the linker were ligated, yielding pET-gfp-SfiI-H6. For insertion of ELP gene, pET-gfp-SfiI-H6 was digested with SfiI, dephosphorylated and purified using a microcentrifuge spin column kit. The E9, E18, E36, E72 and E144 genes were excised from the pUC19 vector by digestion with PflMI and BglI, the excised genes and the linearized vectors were purified, ligated, and transformed into XL1-Blue cells, respectively, and screened as described above. Figure 17 shows the digested GFP-ELP gene variants in agarose gel.

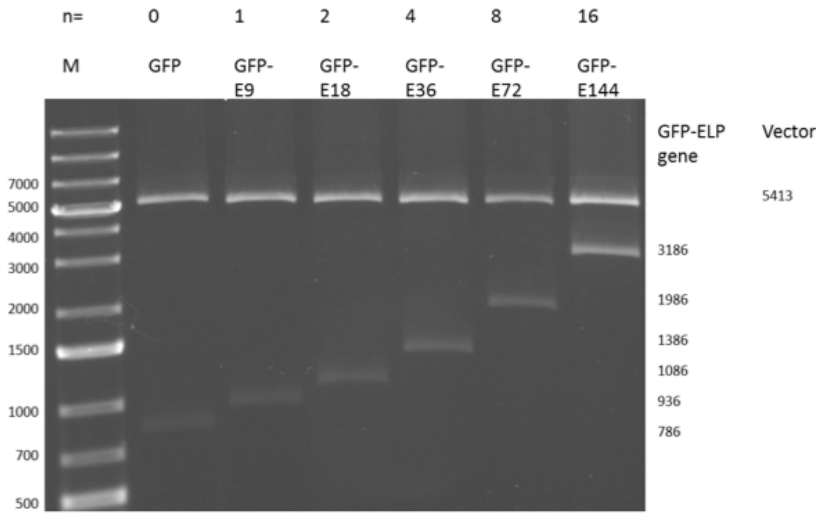

FIGURE 17. **AGAROSE GEL ELECTROPHORESIS OF GFP-ELP GENES**. pET-25b(+) vectors containing the gfp-elp genes were digested with XbaI and EcoRI and separated on a 0.8% agarose gel. Ethidium bromide staining was used to visualize DNA bands. Restriction enzyme digestion produced a linear vector of 5413bp and a gfp-elp gene fragment (size in bp is shown on the right). n represents the number of monomers with 10 pentapeptide repeats; GFP (green fluorescent protein); E means glutamic acid; 9-144 represent amount of charges in respective ELP; M represents a polynucleotide size standard.

Protein expression and purification

E.coli BLR (DE3) cells were transformed with the pET-gfp-SfiI-H6 expression vectors containing the respective elp genes. For protein production, Terrific Broth medium (for 1 L, 12 g tryptone and 24 g yeast extract) enriched with phosphate buffer (for 1 L, 2.31 g potassium phosphate monobasic and 12.54 g potassium phosphate dibasic) and glycerol (4 mL per1 L TB) and supplemented with 100 µg/mL ampicillin, was inoculated with an overnight

starter culture to an initial optical density at 600 nm (OD600) of 0.1 and incubated at 37 °C with orbital agitation at 250 rpm until OD600 reached 0.7. Protein production was induced by a temperature shift to 30 °C. Cultures were then continued for additional 16 h post-induction. Cells were subsequently harvested by centrifugation (7,000 x g, 20 min, 4 ºC), resuspended in lysis buffer (50 mM sodium phosphate buffer, pH 8.0, 300 mM NaCl, 20 mM imidazole) to an OD600 of 100 and disrupted with a constant cell disrupter (Constant Systems Ltd., Northands, UK). Cell debris was removed by centrifugation (40,000 x g, 90 min, 4 ºC). Proteins were purified from the supernatant under native conditions by Ni-sepharose chromatography. Product-containing fractions were pooled and dialyzed against ultrapure water and then purified by anion exchange chromatography using a Q HP column. Protein-containing fractions were dialyzed extensively against ultrapure water. Purified proteins were frozen in liquid nitrogen, lyophilized and stored at -20 ºC until further use.

Protein Characterization

The concentrations of the purified GFP-ELP fusion proteins were determined by measuring absorbance at 280 nm using a spectrophotometer (SpectraMax M2, Molecular Devices, Sunnyvale, CA). Protein purity was determined by sodium dodecyl sulfate polyacrylamide gel electrophoresis (SDS-PAGE) on a 10% polyacrylamide gel. Afterwards, gels were stained with coomassie staining solution (40% methanol, 10% glacial acetic acid, 1 g/L Brilliant Blue R250). Photographs of the gels after coomassie staining (shown in Fig.4) were taken with a LAS-3000 Image Reader (Fuji Photo Film (Europe) GmbH, Dusseldorf, Germany).

Fluorescent spectra of GFP and GFP-ELPs

GFP concentration in phosphate buffer solution (PBS) was determined by measuring absorbance at 488 nm. Volumes were adjusted with PBS until absorbance at 488 nm was between 0.82 and 0.85. Samples were diluted ten times in PBS for fluorescence measurements. Fluorescence spectra were recorded upon excitation at 488 nm (Figure 5c). Measurements were carried out in triplicates and average fluorescence values were corrected for differences in absorbance according to:

$$RFUcorr = RFUmeas \cdot 0.84 / abs488,$$

with RFUcorr being the corrected relative fluorescence unit (RFU), RFUmeas the measured RFU, and abs488 the measured absorbance at 488 nm of the ten

times concentrated solution. UV absorption and fluorescence spectra of GFP-ELPs were recorded on a fluorimeter (SpectraMax M2, Molecular Devices, Sunnyvale, CA).

Mass Spectrometry

Mass spectrometric analysis was performed using a 4800 MALDI-TOF/TOF Analyzer in the linear positive mode. The protein samples were mixed 1:1 v/v with sinapinic acid matrix (SIGMA) (100 mg/mL in 70% ACN and 0.1% TFA). Mass spectra were analyzed with the Data Explorer software (version 4.9).

Preparation of GFP-E72-DDAB complexes

GFP-E72-DDAB complex was prepared as described in chapter 2. In brief, 20 nmol of GFP-E72 were dissolved in 100 μL NaCl (100 mM) solution. At the same time, ~3 mole equivalents of cationic DDAB relative to glutamate residues within the ELP were dissolved in an equal volume of ultrapure water. After mixing the precipitate that occurred was collected by centrifugation and was then lyophilized before further characterization. The composition of the GFP-E72-DDAB complex was determined by calculating the [ELP]:[DDAB] ratio as described in chapter 2.

GFP-ELPs-surfactants complexes preparation

GFP-ELP-surfactant complex: GFP-ELP (GFPE9, GFPE18, GFPE36, GFPE72 and GFPE144) aqueous solution (~300 μM) was obtained by dissolving dry GFP-ELPs in 100 mM NaCl aqueous solution. In a second solution made from ultrapure water, the concentration of two mixed surfactants (DOAB:DEAB, DOAB:DDAB and DEAB:DDAB, molar ratio are 7:3, 5:5 and 3:7) were adjusted to 50-100 mM at room temperature. Both the GFP-ELP and surfactants solutions (~5 mol equivalents of surfactant relative to the glutamate residues within ELPs) were mixed together and as a result the insoluble complexes precipitated from the aqueous phase. After centrifugation the water and unreacted surfactants were removed, and finally the complexes were lyophilized overnight before further characterization.

Fluorescence spectra of GFP-ELP-surfactant complexes

Fluorescence measurements of GFP-ELP-surfactant complexes were performed on a Fluorolog 3 (Jobin Yvon Horiba).

TGA and DSC

Thermogravimetric analysis (TGA) and differential scanning calorimetry (DSC) for GFP-ELP-surfactant complexes were carried out using a TA Instruments Q1000 system in a nitrogen atmosphere and with a heating/cooling rate of 5 °C/min.

POM

Polarized optical microscopy (POM) was conducted on a Zeiss Axiophot using the same temperature program as employed for the DSC experiments and it was carried out on samples sandwiched between clean glass microscope slides spaced by a gap of 10 μm.

SAXS and WAXS

Small-angle and wide-angle X-ray scattering (SAXS and WAXS) with heating and cooling systems were performed, as described in chapter 2, by employing a conventional X-ray source with radiation wavelength of $\lambda = 1.54$ Å. For SAXS, a Bruker Nano/microstar instrument was used to obtain small angle scattering profiles, where the sample-to-detector distance was 240 cm. WAXS was carried out by a home-made, rotating-anode–based setup where the sample-to-detector distance was 13 cm.

FF-TEM

Freeze-fractured transmission electron microscopy (FF-TEM) was carried out according to standard protocols[23] and as described in chapter 2. Briefly, it was performed by sandwiching the samples between 2 mm by 3 mm glass planchettes and cooling from the isotropic melt to a selected temperature in the LC range then rapidly quenched to T < -180 °C by immersion in liquid propane, fractured in vacuum at -140 °C, and then coated with 2 nm of platinum deposited at 45° and then with 25 nm of carbon deposited at 90°. After dissolving the liquid crystal, the Pt–C replicas were placed in the TEM (Philips CM10 transmission electron microscope operating at an accelerating voltage of 100 kV). Images were recorded on a Gatan slow-scan CCD camera.

3.5 Bibliography

1. Rariy, R. V. & Klibanov, A. M. Correct protein folding in glycerol. *Proc. Natl. Acad. Sci.* **94,** 13520–13523 (1997).
2. Knubovets, T., Osterhout, J. J., Connolly, P. J. & Klibanov, A. M. Structure, thermostability, and conformational flexibility of hen egg-white lysozyme dissolved in glycerol. *Proc. Natl. Acad. Sci.* **96,** 1262–1267 (1999).
3. Clark, D. S. Characteristics of nearly dry enzymes in organic solvents: implications for biocatalysis in the absence of water. *Philos. T. Roy. Soc. B* **359,** 1299–1307 (2004).
4. van Rantwijk, F. & Sheldon, R. A. Biocatalysis in ionic liquids. *Chem. Rev.* **107,** 2757–2785 (2007).
5. Kodera, Y., Nishimura, H., Matsushima, A., Hiroto, M. & Inada, Y. Lipase Made Active in Hydrophobic Media by Coupling with Polyethylene-Glycol. *J. Am. Oil Chem. Soc.* **71,** 335–338 (1994).
6. Basri, M. *et al.* Synthesis of Fatty Esters by Polyethylene Glycol-Modified Lipase. *J. Chem. Technol. Biot.* **64,** 10–16 (1995).
7. Okahata, Y. & Ijiro, K. A lipid-coated lipase as a new catalyst for triglyceride synthesis in organic solvents. *J. Chem. Soc., Chem. Commun.* 1392–1394 (1988).
8. Mattos, C. & Ringe, D. Proteins in organic solvents. *Curr. Opin. Struc Biol.* **11,** 761–764 (2001).
9. Min, Y., Akbulut, M., Kristiansen, K., Golan, Y. & Israelachvili, J. The role of interparticle and external forces in nanoparticle assembly. *Nat. Mater.* **7,** 527–538 (2008).
10. Liu, L., Bagal, D., Kitova, E. N., Schnier, P. D. & Klassen, J. S. Hydrophobic Protein−Ligand Interactions Preserved in the Gas Phase. *J. Am. Chem. Soc* **131,** 15980–15981 (2009).
11. Perriman, A. W., Cölfen, H., Hughes, R. W., Barrie, C. L. & Mann, S. Solvent-free protein liquids and liquid crystals. *Angew. Chem. Int. Ed. Engl.* **48,** 6242–6246 (2009).
12. Perriman, A. W. *et al.* Reversible dioxygen binding in solvent-free liquid myoglobin. *Nat. Chem.* **2,** 622–626 (2010).
13. Ayres, L., Vos, M., Adams, P., Shklyarevskiy, I. O. & Van Hest, J. Elastin-based side-chain polymers synthesized by ATRP. *Macromolecules* **36,** 5967–5973 (2003).

14. del Mercato, L. L. *et al.* Amyloid-like Fibrils in Elastin-Related Polypeptides: Structural Characterization and Elastic Properties. *Biomacromolecules* **9,** 796–803 (2008).
15. Stanley, C. B. & Strey, H. H. Electrostatically driven self-assembly of hybrid elastin–DNA liquid crystals. *Soft Matter* **4,** 241–244 (2008).
16. Kolbe, A. *et al.* De Novo Design of Supercharged, Unfolded Protein Polymers, and Their Assembly into Supramolecular Aggregates. *Macromol. Rapid Commun.* **32,** 186–190 (2010).
17. Meyer, D. & Chilkoti, A. Genetically encoded synthesis of protein-based polymers with precisely specified molecular weight and sequence by recursive directional ligation: examples from the elastin-like polypeptide system. *Biomacromolecules* **3,** 357–367 (2002).
18. Santhosh Babu, S. *et al.* Solvent-Free Luminescent Organic Liquids. *Angew. Chem. Int. Ed. Engl.* **51,** 3391–3395 (2012).
19. Michinobu, T. *et al.* Structural Requirements for Producing Solvent-Free Room Temperature Liquid Fullerenes. *Langmuir* **29,** 5337–5344 (2013).
20. Sato, K. Crystallization behaviour of fats and lipids — a review. *Chem. Eng. Sci.* **56,** 2255–2265 (2001).
21. Broer, D. J., Bastiaansen, C. M. W., Debije, M. G. & Schenning, A. P. H. J. Functional Organic Materials Based on Polymerized Liquid-Crystal Monomers: Supramolecular Hydrogen-Bonded Systems. *Angew. Chem. Int. Ed. Engl.* **51,** 7102–7109 (2012).
22. Ponomarenko, E. A., Waddon, A. J., Bakeev, K. N., Tirrell, D. A. & MacKnight, W. J. Self-assembled complexes of synthetic polypeptides and oppositely charged low molecular weight surfactants. Solid-state properties. *Macromolecules* **29,** 4340–4345 (1996).
23. Severs, N. J. Freeze-fracture electron microscopy. *Nat. Protoc.* **2,** 547–576 (2007).